NUKLEONIKA 2019;64(1):31–38
doi: 10.2478/nuka-2019-0004

ORIGINAL PAPER

Effect of electronic cigarette (EC) aerosols on particle size distribution in indoor air and in a radon chamber

Hyam Nazmy Khalaf, Mostafa Y. A. Mostafa, Michael Zhukovsky

Abstract. Particle size distribution is an important factor governing whether aerosols can be deposited in various respiratory tract regions in humans. Recently, electronic cigarette (EC), as the alternative of tobacco cigarette, has become increasingly popular all over the world. However, emissions from ECs may contribute to both indoor and outdoor air pollution; moreover, comments about their safety remain controversial, and the number of users is increasing rapidly. In this investigation, aerosols were generated from ECs and studied in the indoor air and in a chamber under controlled conditions of radon concentration. The generated aerosols were characterized in terms of particle number concentrations, size, and activity distributions by using aerosol diffusion spectrometer (ADS), diffusion battery, and cascade impactor. The range of ADS assessment was from 10^{-3} μm to 10 μm. The number concentration of the injected aerosol particles was between 40 000 and 100 000 particles/cm^3. The distribution of these particles was the most within the ultrafine particle size range (0–0.2 μm), and the other particle were in the size range from 0.3 μm to 1 μm. The surface area distribution and the mass size distribution are presented and compared with bimodal distribution. In the radon chamber, all distributions were clearly bimodal, as the free radon decay product was approximately 1 nm in diameter, with a fraction of ~0.7 for a clean chamber (without any additional source of aerosols). The attached fraction with the aerosol particles from the ECs had a size not exceeding 1.0 μm.

Keywords: size distribution • ultrafine particles (UFPs) • electronic cigarette (EC) • radioactive aerosols

H. N. Khalaf, M. Y. A. Mostafa✉
Ural Federal University
19 Mira St., 620002 Yekaterinburg, Russia
and Department of Physics
Minia University
El-Minia, Egypt
E-mail: mostafa_85@mail.ru

M. Zhukovsky
Institute of Industrial Ecology UB RAS
20 Sophy Kovalevskoy St., Ekaterinburg 620990, Russia

Received: 11 September 2018
Accepted: 28 December 2018

Introduction

Tobacco smoking causes some millions of people around the world to die annually. These deaths are the outcomes of direct tobacco smoking or are caused by exposure to secondhand smoke [1]. The chemical composition of both mainstream and secondhand smoke is almost identical. However, the total particle concentrations vary greatly [2]. Electronic cigarettes (ECs) are advertised as a healthier alternative to conventional cigarettes, and they are categorized as electronic nicotine delivery systems (ENDS). ECs or ENDS produce an inhaled aerosol instead of smoke, providing an alternative mode of nicotine delivery [3]. They usually consist of a battery, flow sensor, an aerosol generator, and a solution of nicotine (or e-liquid), as shown in Fig. 1 [4]. The battery is designed to vapourize (by heat) a solution of nicotine (e-liquid) and other additives (including propylene glycol, vegetable glycerin, and ad hoc flavouring agents) into an aerosol, which is then inhaled by the user (called vaping) [5, 6]. The propylene glycol released in the vapour is known to be responsible for upper airway irritations [7, 8]. ECs produce a mist of liquid droplets

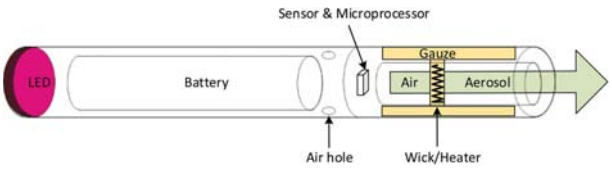

Fig. 1. Typical EC configuration [4].

suspended in the mixture of vapours and air. EC droplets are formed by the condensation of a vapour produced by the heating of the e-liquid, and they contain different proportions of e-fluid constituents and by-products [9].

Although the use of ECs has become increasingly prevalent in recent years, it has become one of the fastest ways to increase the concentration of indoor particles [10]. The particle size distribution of EC aerosols is an important physical property, and reliable measurements are needed for the assessment of respiratory dosimetry, which has not seen wide discussion [11]. Accurate particle size distribution measurements provide a starting point for respiratory tract deposition calculations, although factors other than particle size, such as concentration, chemical composition, and so on, also play a role in regional and total aerosol deposition [11, 12]. Knowledge of the particle size distribution and chemical composition is essential because it determines deposition hotspots and, mainly, the subsequent impact on the human health.

Moreover, since the popularity of ECs has spread only recently, there are no direct studies engaged in the long-term use of ECs and its biological effects on human health [6]. Measurements of particle concentrations and size distributions involve many obstacles and complications because one has to deal with high-concentration aerosol containing volatile compounds. Ingebrethsen *et al*. used spectral transmission to analyse particle concentration and sizes of undiluted EC aerosol [12]. Fuoco *et al*. compared several ECs and conventional tobacco products using Fast Mobility Particle Sizer spectrometer [8]. Results from both studies showed that EC aerosol is highly concentrated (order of 109 particles/cm^3), with particle diameters around 200 nm. Manigrasso *et al*. used a similar experimental setup and the results were implemented in a model for prediction of particle deposition in human respiratory airways [13]. Schripp *et al*. studied indoor air quality in conjunction with EC smoking by placing a volunteer smoker into an 8 m^3 chamber [14, 15].

As is known, radon is the second leading cause of lung cancer after smoke. Therefore, the attachment of radon decay products to EC smoke particles gives an increased risk of lung cancer (as in the case of workers in mines or places with high radon concentrations). Although the question has been extensively discussed, not many systematic studies have been carried out to characterize the system of radon decay products and EC particles. In the past few decades, considerable epidemics have occurred, and hence, knowledge of the health effects of inhalation of air containing both radon decay products and cigarette or EC is essential. Much less effort has been

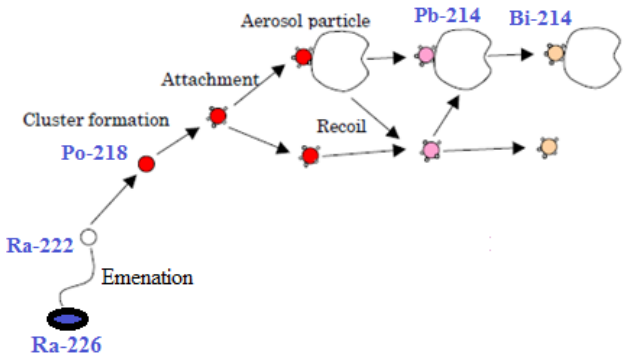

Fig. 2. Radioactive aerosol formation after radon emanation.

focused on the physical aspects of the problem and the effects of environmental factors on the behaviour of radon decay products in the presence of cigarette or EC particles.

Unattached radon decay products are very mobile and, in the presence of aerosols, they are readily attached to the particle surfaces. The rate of attachment is dependent on the size distribution, or diffusion coefficient, of the radon decay products as well as on the aerosol size distribution [16–19]. Both dosimetry assessments and the correct interpretation of the results of measurements of the volumetric activity of radioactive aerosols in the ambient air are necessary. The basic processes involving radon decay products and aerosols are shown in Fig. 2.

Because ECs are becoming increasingly popular nowadays, it is very important to study their properties and evaluate their potential health threats. In this paper, we measured the concentrations and size distributions of the particles emitted by commonly available ECs. Moreover, we aimed to undertake detailed studies in order to understand the relationship between the attached and unattached fractions of radon progeny in the presence of EC particles in the ambient air or under high radon concentrations. This study includes measurements of the size and activity distributions of aerosol particles under controlled conditions of EC particles in the indoor air and with relatively high radon concentrations in a special radon chamber. The number size distribution of particles in the ambient air or with the aerosols generated from ECs is measured with aerosol diffusion spectrometer (ADS). Activity distribution of ultrafine particles (UFPs) is monitored using a screen diffusion battery (SDB). The radioactive aerosol-attached particles are size-fractionated with a cascade impactor. Fractionation of the aerosol allows the determination of the dependence of aerosol particle size on the attachment rate.

Materials and methods

Free radon decay products that have not become attached to aerosol particles exist in a cluster form, having sizes in the nanometer diameter range. To measure their activity distribution or diffusion coefficient spectrum, an SDB can be used. The battery

is not a differential-type collection device; therefore, the activity data on the screens must be convoluted to attain the size distributions. Therefore, the battery is an excellent separator for activity that is free (or in the form of clusters) from activity that is attached to aerosols. The concentrations of radon decay products determined from a diffusion battery with backup filter samples allow us to calculate the attachment rates experimentally.

To determine the activity distributions of the radon progeny that have become attached to the EC aerosols, a cascade impactor (AIP-2) is used. The particle collection stages of conventional impactors accumulate particle deposits in discrete areas immediately under the impaction jets. The collection stages of the impactor move to attain uniform particle deposition across the collection surface, a requirement for the subsequent analysis of alpha activity.

Experiments were carried out in an indoor air laboratory and in a standard chamber under controlled conditions of radon concentration [20, 21]. Additional aerosol particles were injected using ECs. Aerosol was released from the e-cigarette using a smoking machine with a flow rate of 1 L/min. The aerosol parameters were measured continuously with ADS (flow rate 0.5 L/min) in the range from 10^{-3} μm to 10 μm. More details about the ADS can be found in previous papers [21–23].

The instruments used in this work were a diffusion battery for determining the active median thermodynamic diameter (AMTD), a cascade impactor for determining the active median aerodynamic diameter (AMAD), and an ADS to give the aerosol concentration, number, surface area, and mass size distributions.

The SDB had been developed with 10 elements for measuring the radioactive aerosol size distribution in the range from 0.1 nm to 100 nm. Table 1 presents the parameters of the used screen. The working range of the battery with 10 wire screens was in the range d_{50}% from 1.5 nm to 10.8 nm. The overview and construction of the diffusion battery is shown in Fig. 3.

Table 1. Parameters of the screen used in the SDB

Property	Value
Width of cell expansion	100 μm
Wire thickness	65 μm
Mesh thickness	130 μm
Net weight	0.69 g
Mesh diameter	50 mm
Density of the mesh material	8.5 g/cm^3

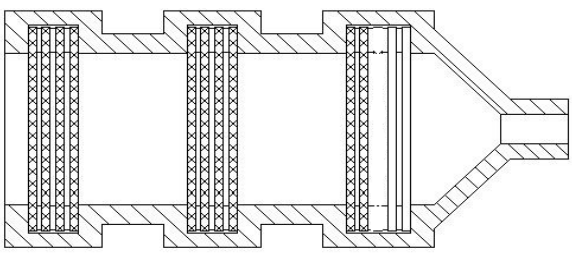

Fig. 3. Appearance and construction of the diffusion battery.

Fig. 4. The external and internal views of the AIP-2 cascade impactor.

The cascade impactor AIP-2 consists of five cascades made of stainless steel with holes of different sizes, and the 50% cutoff diameters of the cascade impactor AIP-2 at air flow rate of 30 L/min are 0.8, 1.6, 5, 8.3, and 23.3 μm [24]. Figure 4 illustrates the external and internal characteristics of the AIP-2 cascade impactor.

The alpha activities on the elements of the diffusion battery and cascade impactors were subsequently measured by a scintillation alpha radiometer (BDPA-01) for 30 min after finishing the sampling process (5 min); the measurement time of a single wire screen or every cascade plate was nearly 2 min. Then, the equivalent equilibrium concentration of radon at the moment of finishing of the sampling was calculated by the modified Kuznets method [25].

The BDPA-01 alpha radiometer was designed to measure low levels of alpha radiation based on the use of a 60-mm-diameter ZnS (Ag) scintillation detector and a photoelectric multiplier. This detector works with an ATecxh program. This program allows the estimation of the flux density, alpha particle fluency, and counting rate, with statistical error and their thresholds. The detector efficiency is 15% for Pu-239 line with 20% uncertainty. For each screen of diffusion battery, plate of impactor, and backup filter used, the efficiency was comparable with that using standard high-purity germanium detector [26, 27]. Therefore, the absolute alpha activity on the wire screen or the cascade impactor plate can be easy calculated. For example, the counting rate recorded by the scintillation alpha radiometer (BDPA-01) for the first wire screen was (10 ± 12)%; for the second, the rate was (3 ± 12)%; and for the last screen (no. 20), which was the absolute alpha activity on

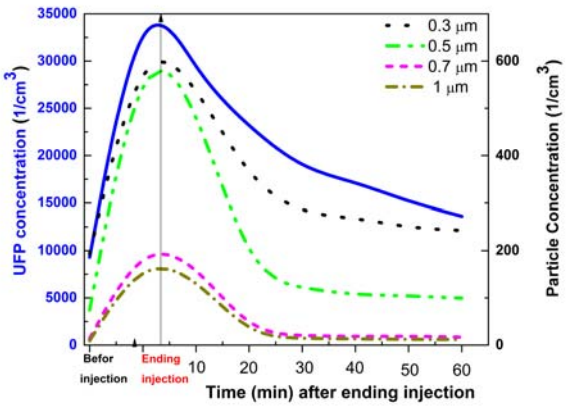

Fig. 5. Aerosol particle concentrations for different sizes determined using ADS before, at the ending of, and after ending aerosol injection from electronic cigarettes.

the wire screen, the rate was (0.25 ± 12)%. The absolute activity can be directly calculated using the alpha efficiency of the used screen (0.075 for brass screen type). The same is the situation for the impactor plate.

The activity distributions were estimated from the alpha energy spectrum analysis of the SDB modes obtained by using a mathematical method, namely, the expectation-maximization method of Maher and Laird (EMM) [28, 29].

Results and discussion

Particle size distribution in indoor air

The particle concentrations and the indoor aerosol size distributions before using the EC in the experimental laboratory room and after injection of the mainstream aerosol particles with the EC were determined by using ADS, as shown in Fig. 5. It presents the concentrations of particles of different sizes – ranging from ≤0.02 μm (UFPs) to 1 μm – before and after smoke injection with the ECs. The maximum concentrations of the UFPs and the fine particles are clear at the end of the injection process. The concentration of UFPs in the indoor ambient air (before injection) is ~9.3 k particles/cm^3, whereas the maximum concentration of UFPs was approximately 39 k particles/cm^3 after aerosol injection by the EC. The particles in the size ranges of 0.3–0.5 μm ranged from tens to some hundreds of particles per cubic centimetre, whereas particles of sizes 0.7 and 1.0 μm are nearly absent before injection and not more than 200–300 particles/cm^3 were present after injection. The concentrations of 0.7 and 1.0 μm particles reached the maximum and then decayed simultaneously with each other. From the figure also, it is observed that the UFPs have a long half-life unlike particles of other sizes: not more than 1 h for particles of size 0.5 μm, and only 30 min for those of size 1 μm.

The different size distributions (number, surface area, and mass) are shown in Fig. 6. The particle size distributions are presented for indoor aerosol (laboratory room) before and after the injection of the mainstream aerosol particles with EC at time intervals of 15, 30, and 60 min after aerosol injection. The particle number and surface area distributions have main mode with number median diameter (NMD) of 89 nm and surface median diameter (SMD) of 124 nm, respectively, with the same geometric standard division (GSD) of 1.5 nm. On the other hand, the mass size distribution has a bimodal distribution of aerosol particles, with two mass median diameters (MMDs) ~120 nm and ~2500 nm and GSD values of 1.4 nm and 1.6 nm, respectively.

It is clear from Fig. 6 that there is an effect of aging on the different size distributions of aerosols in the laboratory air after aerosol injection. As example, the highest mode at 15 min after injection is 58 nm for the NMD and 104 nm for the SMD, which are smaller than the main mode of the background

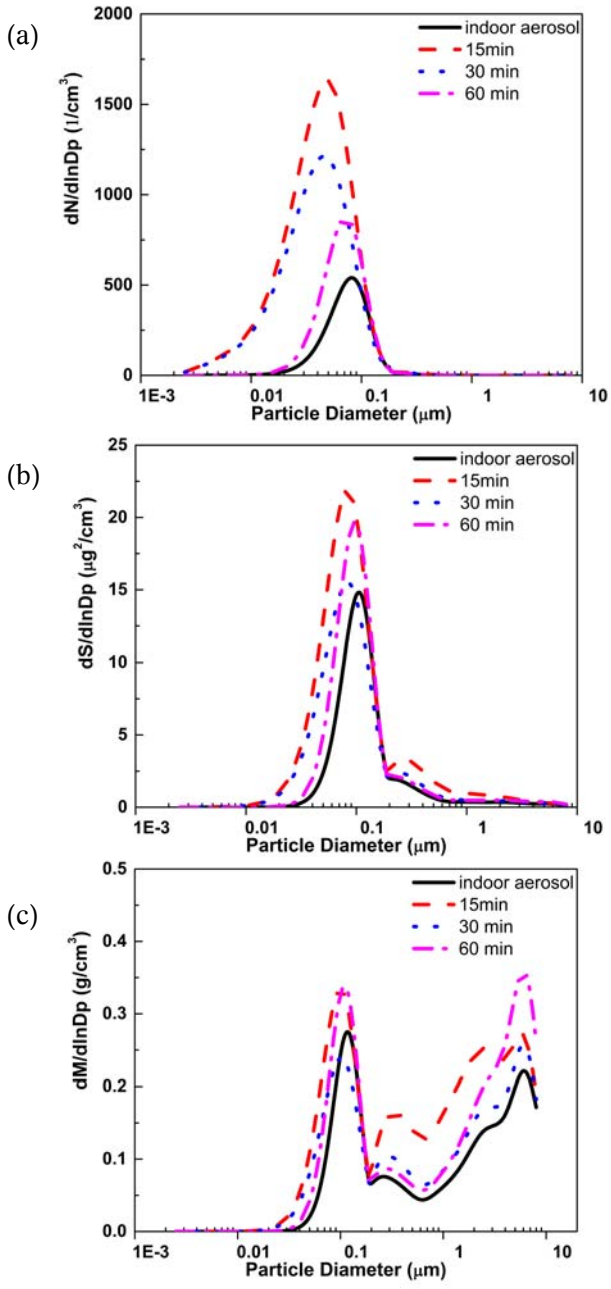

Fig. 6. The number (a), surface area (b), and mass size distributions (c) of the injected aerosol particles as a function of time after aerosol injection.

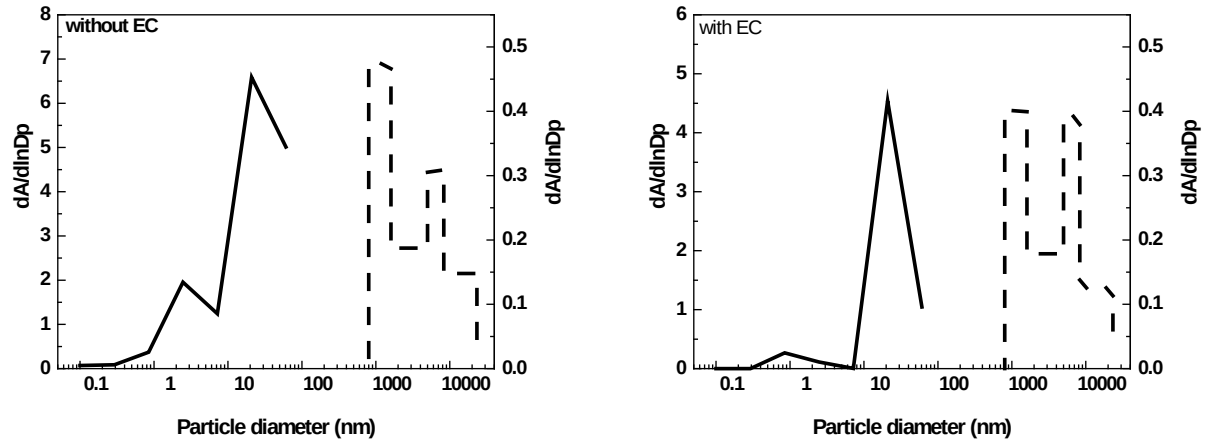

Fig. 7. The active particle size distribution without and with ECs in the indoor air.

(89 nm and 124 nm, respectively), but the GSD increased from 1.5 to 1.7 nm. The shrinking of the particle number distribution can be attributed to the evaporation of the particles under ideal conditions.

The active particle size distribution without and with the EC smoke in the indoor air was measured with the diffusion battery and AIP-2. Figure 7 presents the activity distribution of the aerosol particles in the indoor air without and with smoke. Generally, there is no change for the particles in the diffusion battery size range ≤100 nm. Furthermore, for the AIP-2 impactor size range of 0.8–23 μm, no change was observed. These results are because the indoor air activity is too small, nearly equal to the considered background.

Particle size in the radon chamber

The concentrations of the fractional sizes of aerosol particles before and after aerosol injection were measured continuously in experiments with an ADS instrument connected to the radon chamber. For these experiments, the loss of aerosol to the chamber walls was inconsequential in the determination of the attachment rate of the radon decay products to the aerosol. The measured deposition rates also include any decrease in particle concentration due to coagulation of the aerosol with itself. Thus, coagulation is a significant factor in these measurements, as explained in Fig. 8.

Figure 8 represents the concentrations of particles according to the measurements with ADS. The maximum concentration of UFPs is approximately 10^5 particles/cm^3, while the maximum concentrations of particles in the sizes of approximately 0.3, 0.5, 0.7, and 1 μm are found to be 66, 217, 176, and 302 particles/cm^3, respectively. The maximum concentration of UFPs was reached directly after ending aerosol injection with ECs.

In the radon chamber, the range that showed a marked change of concentration after injection of the aerosol particles was from 2 μm to 7 μm. Aerosols generated by cigarette smoke are likely to be larger in size than those found in the normal ambient air [30, 31]. The larger smoke particles with far greater surface areas would be expected to predominate during collection and determination of unattached radon daughter activity. Furthermore, since the smoke particles constitute a liquid aerosol, the behaviour of attachment and alpha recoil may differ from that expected for aerosols consisting of solid particles. It is suspected that the smoke aerosol would lead to altered deposition pattern and amounts of activity within the respiratory system.

In Fig. 9, for a clean radon chamber, the NMD and the GSD are 119 nm and 1.42 nm, respectively, while the mass and the surface median diameters

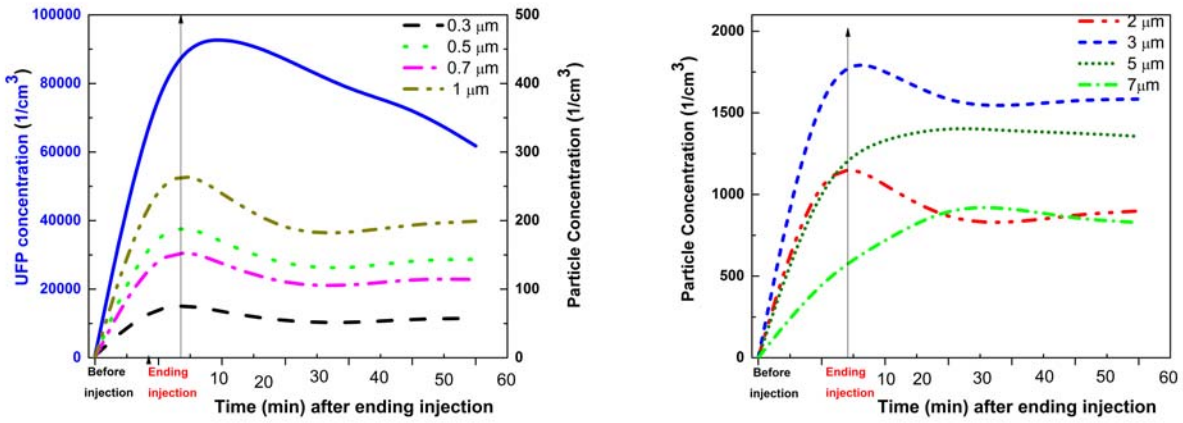

Fig. 8. Concentrations of the aerosol particles of different sizes determined using ADS before and after aerosol injection from electronic cigarette.

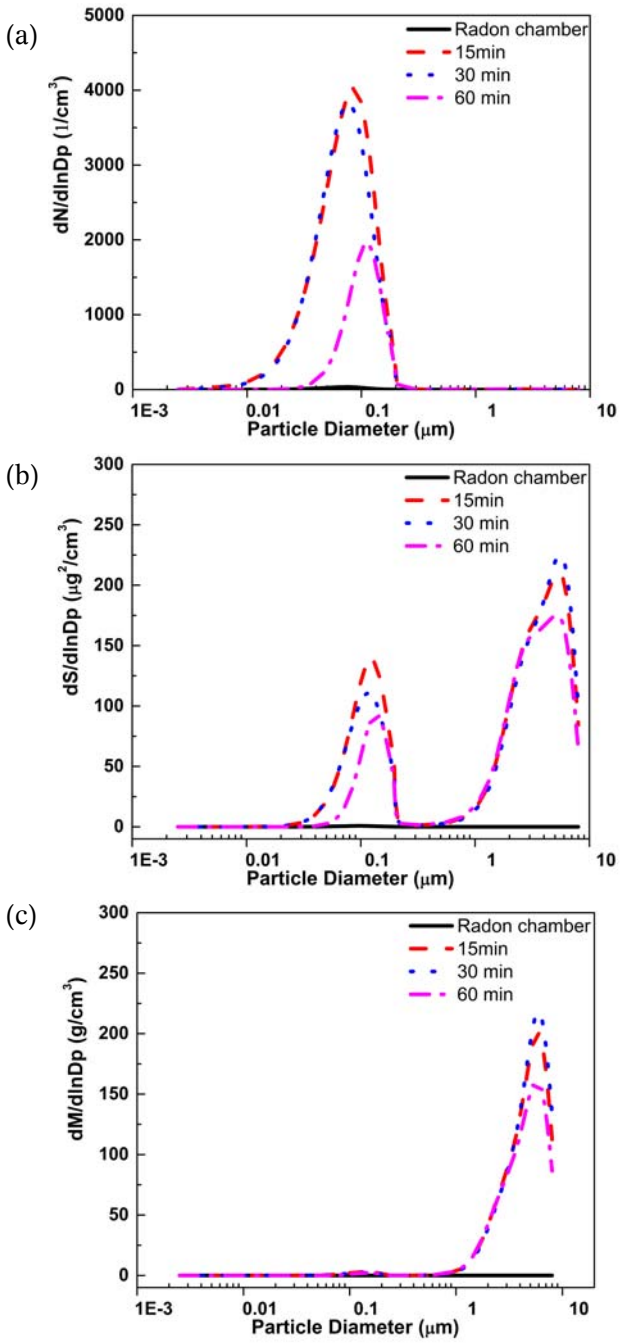

Fig. 9. The number (a), surface area (b), and mass size distributions (c) of the injected aerosol particles as a function of time after aerosol injection.

(MMD and SMD) are 162 nm and 145 nm, respectively, with GSDs of 1.5 nm and 1.34 nm, respectively. At 15 min after aerosol injection with EC, it is clear that for a specific surface area, there are two modes at approximately 120 nm (GSD = 1.39 nm), while the median diameter of the coarse mode is 4.11 μm (GSD = 1.71 μm). At 60 min, NMD is 113 nm, with GSD = 1.38 nm, and for a specific surface area, there are also two modes at approximately ~133 nm (GSD = 1.29 nm) and 3.85 μm (GSD = 1.71 μm). With time, the concentration reduces step by step back to the levels of the clean radon chamber.

The active particle size distribution was measured simultaneously with aerosol size distribution and concentration. The time span between the introduction of the EC smoke and the diffusion battery sampling was 1 h. This was found experimentally to be sufficient for the ingrowth of the nuclide on the new population of particles. It is worth noting that the measurements of the active particle size spectrum were performed not earlier than 30 min after the EC smoke was introduced. For at least 1 h after the EC smoke was introduced, the active particle size spectrum remained unchanged as a result of the still-high concentration of EC smoke in the radon chamber.

The active particle size distribution was measured with and without EC smoke in the radon box (Fig. 10). The effect of EC smoke on the unattached fraction in the chamber can be expressed as the ratio of the unattached fraction without EC smoke in the chamber to that with smoke.

Most of the activity is present on the aerosol, which is depicted in the maximum size interval of the diffusion battery size array. About 90% of the activity has attached to the aerosol. However, the diffusion battery is not capable of resolving the activity attached to the aerosol because the aerosol distribution is greater than the useful range of the battery.

Therefore, the activity attached to aerosol is readily resolved by sampling with the cascade impactor. All distributions are distinctly bimodal, clearly illustrating the free radon decay products

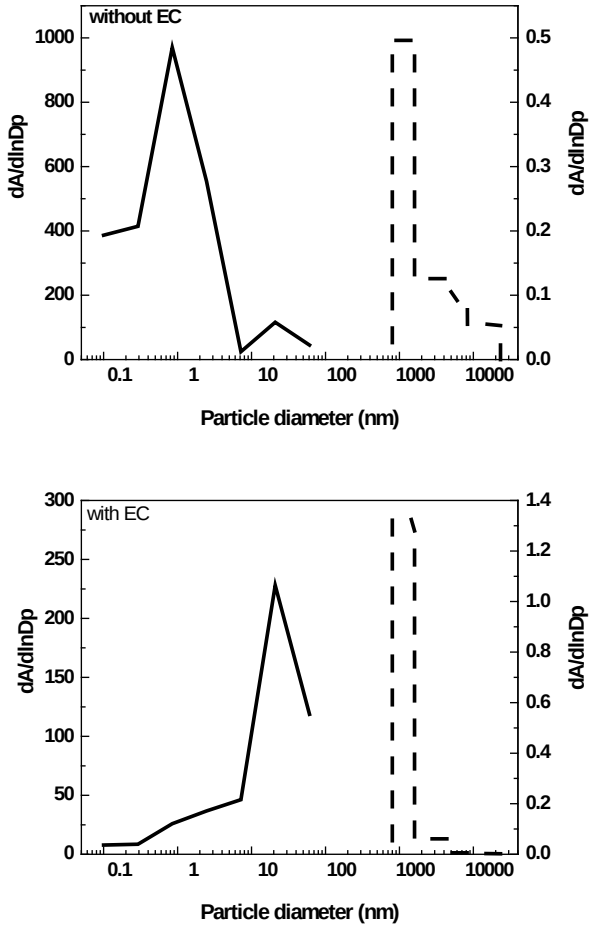

Fig. 10. Active particle size distribution with and without ECs in the radon chamber.

of approximately 1 nm diameter and the attached fraction on the aerosol particles of nearly 1.0 μm diameter range. The free radon decay product mode remains extremely sharp as in the case of experiment with no aerosol. Now that the aerosol is present, the majority of the activity has moved from the free mode to the aerosol mode.

In a study by Morawska *et al*. on radon attachment to cigarette smoke, median diameters of 1.19 nm for the free progeny and 0.1 μm for the aerosol were determined [32]. In contrast to the smoke aerosols, the activity distribution for the ambient aerosol has an activity median diameter of 0.12 μm and a standard deviation of 1.9 μm. The ^{214}Pb and ^{214}Bi decay products (not shown) have similar distributions, with the exception that, in the case of presence of smoke, they have even more activity associated with the smoke particles.

From the here-in presented results, it should be noted that the active particle size distribution was always bimodal and both peaks were relatively narrow. These findings agree with data from the literature. A bimodal distribution for the active particles was found in most of the cases when the distribution was determined as a result of direct measurements, even for high aerosol concentrations. The minor mode was usually centred on 1 nm [33, 34] and the major mode, which varied with the characteristics of indoor aerosol, was in the range of 100–150 nm [33]. In contrast, the radon decay product distributions calculated by applying the attachment theory to data on aerosol distribution and concentrations are more often unimodal.

Conclusion

In the indoor air, the concentrations of particles generated by the EC are marked at different sizes, ranging from ≤0.02 μm to 1 μm, whereas in the radon chamber, the range that shows a marked change of concentration is the UFP fraction, ranging from 2 to 7 μm; this may be due to the coagulation of the aerosol with itself.

Activity distributions indicate distinct bimodal size distributions, with modes corresponding to the free radon decay products and the moieties that have attached to the EC smoke particles. Activity of the free radon decay products occurs is determined at about 1 nm in diameter and is nearly of monodisperse nature. Activity of the attached radon decay products, occurring in the submicron size range between 0.1 and 0.4 μm diameter, corresponds to the distribution of the EC smoke particles and shows a heterodisperse nature. The radon daughter activity attached to the EC smoke aerosol was found to be attached to somewhat larger particles. The attachment rate of the radon decay products to the smoke aerosol in a static environment was compared to that with induced turbulence. Although the deposition rate of the free radon decay products to the box walls increased substantially, no significant increases in attachment rate of the radon decay products to the aerosol particles were found.

References

1. WHO. (2008). *Monitoring tobacco use and prevention policies prevalence of adult tobacco use in the 14 countries that completed the global adult tobacco survey*.
2. WHO. (2004). *Tobacco smoke and involuntary smoking*. (IARC Monographs on the Evaluation of Carcinogenic Risks to Humans, Vol. 83). Lyon: WHO, IARC.
3. Glasser, A. M., Collins, L., Pearson, J. L., Abudayyeh, H., Niaura, R. S., Abrams, D. B., & Villanti, A. C. (2017). Overview of electronic nicotine delivery systems. *Am. J. Prev. Med*., *52*(2), e33–e66. doi: 10.1016/j.amepre.2016.10.036.
4. Brown, C. J., & Cheng, J. M. (2014). Electronic cigarettes: product characterisation and design considerations. *Tobacco Control*, *23*, ii4–ii10.
5. Abul, M., Prasad, S., Liles, T., & Cucullo, L. (2016). A decade of e-cigarettes: Limited research and unresolved safety concerns. *Toxicology*, *365*, 67–75.
6. Grana, R., Benowitz, N., & Glantz, S. A. (2014). E-cigarettes: A scientific review. *Circulation*, *129*, 1972–1986.
7. Wieslander, G., Norbäck, D., & Lindgren, T. (2001). Experimental exposure to propylene glycol mist in aviation emergency training: Acute ocular and respiratory effects. *Occup. Environ. Med.*, *58*, 649–655.
8. Fuoco, F. C., Buonanno, G., Stabile, L., & Vigo, P. (2014). Influential parameters on particle concentration and size distribution in the mainstream of e-cigarettes. *Environ. Pollut.*, *184*, 523–529.
9. Sosnowski, T. R., & Odziomek, M. (2018). Particle size dynamics: Toward a better understanding of electronic cigarette aerosol interactions with the respiratory system. *Front. Physiol.*, *9*, article 853, 1–8. doi: 10.3389/fphys.2018.00853.
10. Ciuzas, D., Prasauskas, T., Krugly, E., Sidaraviciute, R., Jurelionis, A., Seduikyte, L., Kauneliene, V., Wierzbicka, A., & Martuzevicius, D. (2015). Characterization of indoor aerosol temporal variations for the real-time management of indoor air quality. *Atmos. Environ.*, *118*, 107–117.
11. Robinson, R. J., & Yu, C. P. (2001). Aerosol science and technology deposition of cigarette smoke particles in the human respiratory tract deposition of cigarette smoke particles in the human respiratory tract. *Aerosol Sci. Technol.*, *34*, 202–215.
12. Ingebrethsen, B. J., Alderman, S. L., & Ademe, B. (2011). Coagulation of mainstream cigarette smoke in the mouth during puffing and inhalation. *Aerosol Sci. Technol.*, *45*(12), 1422–1428.
13. Manigrasso, M., Buonanno, G., Fuoco, F. C., Stabile, L., & Avino, P. (2015). Aerosol deposition doses in the human respiratory tree of electronic cigarette smokers. *Environ. Pollut.*, *196*, 257–267.
14. Belka, L., Lizal, F., Jedelsky, J., Jicha, M., & Pospisil, J. (2017). Measurement of an electronic cigarette aerosol size distribution during a puff. *EPJ Conf.*, *143*, 02006. DOI: 10.1051/epjconf/201714302006.
15. Schripp, T., Markewitz, D., Uhde, E., & Salthammer, T. (2013). Does e-cigarette consumption cause passive vaping? *Indoor Air*, *23*(1), 25–31.
16. Yuness, M., Mohamed, A., AbdEl-hady, M., Moustafa, M., & Nazmy, H. (2015). Effect of indoor activity size

distribution of ^{222}Rn progeny in-depth dose estimation. *Appl. Radiat. Isot.*, *97*, 34–39.
17. Yuness, M., Mohamed, A., Nazmy, H., Moustafa, M., & Abd El-hady, M. (2016). Indoor activity size distribution of the short-lived radon progeny. *Stoch. Environ. Res. Risk Assess.*, *30*(1), 167–174.
18. Mohamed, A., Abd El-hady, M., Moustafa, M., & Yuness, M. (2014). Deposition pattern of inhaled radon progeny size distribution in human lung. *J. Radiat. Res. Appl. Sci.*, *7*(3), 333–337.
19. Mostafa, Y., Mohamed, A., Abd El-hady, M., Moustafa, M., & Nazmy, H. (2015). Indoor activity of short-lived radon progeny as critical parameter in dose assessment. *Solid State Phenom.*, *238*, 151–160.
20. Mostafa, Y. A. M., Vasyanovich, M., Zhukovsky, M., & Zaitceva, N. (2015). Calibration system for radon EEC measurements. *Radiat. Prot. Dosim.*, *164*(4), 587–590.
21. Khalaf, H. N., Vasyanovich, M., Mostafa, M. Y. A., & Zhukovsky, M. (2019). Comparison of radioactive aerosol size distributions (Activity, number, mass, and surface area). *Appl. Radiat. Isot.*, *145*, 95–100.
22. Nazmy, H., Mostafa, M. Y. A., & Zhukovsky, M. (2018). Particle size distribution of e-cigarette aerosols in indoor air. *J. Radiat. Nucl. Appl.*, *3*(2), 111–117.
23. Khalaf, H. N. B., Mostafa, M. Y. A., & Zhukovsky, M. (2018). Radiometric efficiency of analytical filters at different physical conditions. *J. Radioanal. Nucl. Chem*. https://doi.org/10.1007/s10967-018-6347-6.
24. Vasyanovich, M., Mostafa, M. Y. A., & Zhukovsky, M. (2017). Ultrafine aerosol influence on the sampling by cascade impactor. *Radiat. Prot. Dosim.*, *177*(1/2), 49–52.
25. Nazaroff, W. W. (1980). An improved technique for measuring working level of radon daughters in residences. *Health Phys*., *45*, 509–523.
26. Mostafa, Y. A. M., Vasyanovich, M., & Zhukovsky, M. (2016). Prototype of a primary calibration system for measurement of radon activity concentration. *Appl. Radiat. Isot*., *107*, 109–112.
27. Mostafa, Y. A. M., Vasyanovich, M., & Zhukovsky, M. (2017). A primary standard source of radon-222 based on the HPGe detector. *Appl. Radiat. Isot*., *120*, 101–105.
28. Zhukovsky, M., Rogozina, M., & Suponkina, A. (2014). Size distribution of radon decay products in the range 0.1–10 nm. *Radiat. Prot. Dosim.*, *160*(1/3), 192–195.
29. Rogozina, M., Zhukovsky, M., Ekidin, A., & Vasyanovich, M. (2014). Thoron progeny size distribution in monazite storage facility. *Radiat. Prot. Dosim.*, *162*(1/2), 10–13.
30. Biennann, A. H., & Sawyer, S. S. (1995). *Attachment of radon progeny to cigarette-smoke aerosols*. U.S. Department of Energy by Lawrence Livermore National Laboratory. (Contract no. W-740S-ENG-48).
31. Muller, W. J., Scherer, P. W., & Hess, G. D. (1990). A model of cigarette smoke particle deposition. *Am. Ind. Hyg. Assoc. J.*, *51*(5), 245–256.
32. Morawska, L., & Phillips, C. R. (2007). Aerosol science and technology attachment of radon progeny to cigarette smoke aerosol attachment of radon progeny to cigarette smoke aerosol. *Aerosol Sci. Technol.*, *17*(3), 149–158.
33. Tu, K. W., & Knutson, E. O. (1988). Indoor radon progeny particle size distribution measurements made with two different methods. *Radiat. Prot. Dosim.*, *24*(1/4), 251–255.
34. Holub, R. F., Knutson, E. O., & Solomon, S. (1988). Tests of the graded wire screen technique for measuring the amount and size distribution of unattached radon progeny. *Radiat. Prot. Dosim.*, *24*(9), 265–268.